[7] "Circuit arrangement to improve the linearity of an angle-modulated oscillator," Swedish Patent Application, No. 73/089062.
[8] P. Penfield and R. P. Rafuse, *Varactor Applications*. Cambridge, Mass.: M.I.T. Press, 1962.
[9] G. Endersz, Memorandum, L M Ericsson, 7546/Ue 2028, 1972.
[10] I. Török, M.S. thesis, Technical University of Budapest, Budapest, Hungary, 1966.

Gunn-Effect Amplifiers for Microwave Communication Systems in *X*, *Ku*, and *Ka* Bands

J. G. DE KONING, MEMBER, IEEE, R. E. GOLDWASSER, R. J. HAMILTON, JR., MEMBER, IEEE, AND F. E. ROSZTOCZY

***Abstract*—This paper describes the design and performance of small-signal stable multistage Gunn-effect reflection-type amplifiers for communication systems in *X*, *Ku*, and *Ka* bands. A single-stage design approach is developed, based on measured small-signal *Z* parameters of the Gunn diodes. This technique is then applied to a microstrip medium at lower frequencies (*X* and *Ku* bands) and to a coax/waveguide hybrid structure at *Ka* band. Performance of a two-stage amplifier is described in the bands 11.7 to 12.2 GHz and 14.0 to 14.5 GHz. In high *Ka* band, performance of both a two- and a four-stage amplifier is presented.**

I. INTRODUCTION

EARLY experiments with low n_0L product ($n_0L < 5 \times 10^{11}$ cm^{-2}) GaAs Gunn devices resulted in low-power narrow-band reflection amplification at microwave and millimeter wave frequencies [1], [2]. Since the first observation of the stabilization of highly doped Gunn devices [3], wide-band Gunn-effect amplifier prototypes in *C*, *X*, and *Ku* band have been built [4]–[8].

Multistage Gunn-effect amplifiers for FM–CW communication systems have been reported, and 1 W at 30 dB gain in *X* band and 0.5 W in *Ku* band have been achieved [9]. These waveguide cavity amplifiers exhibited less than 350-MHz bandwidth, time-delay variations of 5 ns over 200 MHz in *X* band, and considerable gain expansion. Low-power narrow-band (<0.2 GHz) millimeter wave amplification at 34 GHz has been reported using supercritical GaAs and InP devices [10], [11]. Recently, a GaAs Gunn-effect amplifier with 110-mW saturated power output at 35 GHz was described [12]. The single-stage amplifier had a gain of 13 dB and a 3-GHz 3-dB bandwidth.

The objective of this paper is to describe recent advances in Gunn-effect amplifiers designed for microwave communication systems at frequencies ranging from *X* to *Ka* band. Particular attention has been given to achieve minimal variations of gain and phase, intermodulation distortion, and AM–PM conversion. The physics and the impedance characteristics of Gunn diodes from *C* to *Ka* band are discussed, followed by a description of generalized single-stage amplifier design approach. The actual physical design of certain multistage communication amplifiers in *X*, *Ku*, and *Ka* bands will be described.

Manuscript received February 2, 1974; revised June 16, 1974.
The authors are with Varian Associates, Palo Alto, Calif. 94303.

II. GUNN DIODE CHARACTERISTICS AND DISCUSSION OF IMPORTANT PARAMETERS

At sufficiently high electric fields, GaAs exhibits external negative resistance which is caused by a local negative differential mobility inside the crystal. This negative differential mobility can lead to a variety of external appearances, one of which is the stable negative resistance mode.

In the stable negative resistance mode, the diode exhibits an RF impedance with a negative real part for frequencies close to the transit time frequency. The frequency range over which negative resistance is observed is of the order of 1 octave. A stable Gunn diode can be utilized to form an oscillator or a stable reflection amplifier, depending upon the circuit configuration.

In general, the diode parameters required for optimization of power, bandwidth, noise, and stability in an amplifier are very similar to those required for a wide-band oscillator with a similar output power and efficiency. The same diode parameters which lead to wide-band tunability also lead toward stability. Since stability in a realizable circuit is the first criterion, one designs to achieve that characteristic. Generally, n_0L products less than 2×10^{12} cm^{-2} and flat, uniform doping profiles throughout the active layer are preferred.

The package parameters are of critical importance. A micropill package with ceramic dimensions of 0.030 in outer diameter and 0.012 in height has been utilized for the

wide-band Gunn diodes. This package provides a capacity of 0.1 pF and a series inductance of approximately 0.1 nH. These low package parasitics are necessary to obtain a good amplifier design.

The impedance characteristics of stable Gunn diodes have been measured utilizing an automated network analyzer. The diodes are imbedded in a suitable broad-band low-reactance circuit and the dc bias is increased until stable gain is observed. Stable operation is obtained at dc voltages of 2 to 3 times the threshold voltage of the diode. The measurement fixture consists of a section of coaxial line (usually 50 Ω) with the Gunn diode terminating the line. The impedance matrix of the circuit is first determined using three known passive terminations at the diode port.

In the lower frequency bands, *C*, *X*, and *Ku*, the three known terminations are all lumped elements; namely, a short circuit and two known capacitors. The result of this is a full characterization of the circuit at the radial mode reference plane, which is defined by the circumference of the diode package. At higher frequencies, where it becomes more difficult to obtain lumped elements, three offset coaxial shorts are substituted for the active device. At these frequencies, the circuit is then characterized at the TEM reference plane at the end of the center conductor.

The Z matrix for a reciprocal passive 2-port circuit is

$$Z = \begin{bmatrix} Z_{11} & Z_{12} \\ Z_{12} & Z_{22} \end{bmatrix}. \tag{1}$$

The elements of the matrix are determined by solving the set of three simultaneous equations that relate the circuit input impedances to the known load impedances at the diode port. These equations are

$$Z_{IN_i} = Z_{11} - Z_{12}^2/(Z_{22} + Z_{L_i}) \tag{2}$$

where Z_{IN_i} $(i = 1,2,3)$ are the input impedances for Z_{L_i} $(i = 1,2,3)$, the three known loads at the diode port. The input impedances are determined from the reflection coefficient which is measured either on the network analyzer in the case of the three lower bands or with slotted-line techniques above *Ku* band. The three equations may then be solved to yield Z_{11}, Z_{22}, and Z_{12}^2.

Once this Z matrix is obtained, the diode impedances can be directly determined since the diode impedance can be calculated from the equation:

$$Z_d = Z_{12}^2/(Z_{11} - Z_{IN}) - Z_{22} \tag{3}$$

where Z_d is the diode terminal impedance, Z_{11}, Z_{22}, Z_{12}^2 are the previously determined circuit elements, and Z_{IN} equals the input impedance as determined from the measured active reflection coefficient.

The negative of the terminal impedance data of typical Gunn amplifier diodes in *C*, *X*, *Ku*, *K* and *Ka* bands is presented on the Smith chart in Fig. 1. Operating currents are typically 0.6 to 0.8 A. The doping density, active length, n_0L product, threshold voltage, operating voltage,

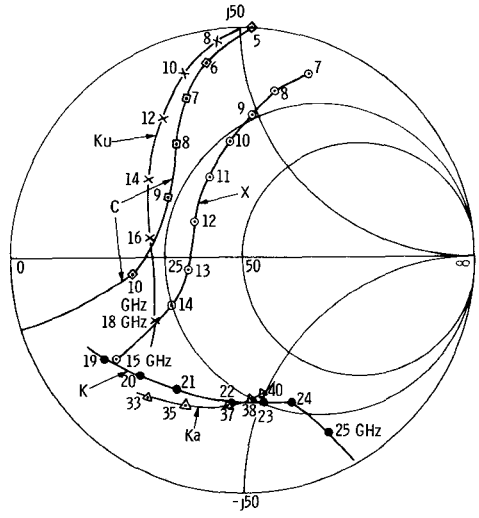

Fig. 1. Smith chart representation of the negative of the Gunn-diode terminal impedances $(-Z_d)$ in *C* through *Ka* bands. The reference plane for *C*, *X*, and *Ku* bands is the radial mode "plane" defined by the circumference of the diode; whereas in *K* and *Ka* bands, the reference is TEM at the end of the coaxial line center conductor in the test fixture.

TABLE I
TYPICAL GUNN-DEVICE CHARACTERISTICS FOR *C* THROUGH *Ka* BANDS

Frequency Band	n_0(x10^{15}cm^{-3})	L (μm)	n_0L(x10^{12}cm^{-2})	V_{th} (V)	V_{op} (V)	I_{op} (A)
C	0.4	13.5	0.54	5.6	16.1	0.6
X	2.3	8.1	1.86	2.77	9.1	0.5
Ku	2.3	6.2	1.43	2.5	8.0	0.6
K	3.1	4.2	1.30	2.1	6.3	0.8
Ka	6.0	2.5	1.50	1.5	5.1	0.8

Note: Comparison of calculated and observed negative resistance bandwidths. The transit time frequency f_T is calculated from the active length L in Table I and assuming a carrier velocity of 1×10^7 cm/s, the calculated negative resistance bandwidth is an octave band centered about f_T.

and current for the various diodes are shown in Table I. As can be seen from Table I, the n_0L product of all diodes is below 2×10^{12} cm^{-2}. Referring to Fig. 1, negative resistance is observed over instantaneous bandwidths of 1 octave or greater, centered about the transit time frequency f_T except for the *Ka* band diode, for which quantitative impedance characteristics are not known above 40 GHz at this time. However, oscillator data for similar devices show that negative resistance extends to well beyond 40 GHz.

The reactive part of the impedance of *C*-, *X*-, and *Ku*-band diodes is capacitive over most of their operating frequency range, while that of the *K*- and *Ka*-band diodes is inductive. This is due to the package parasitics. The real part of the diode impedance is less than -35 Ω for all diodes shown, and the negative Q's range from -1.9 to -2.8, assuming the diodes are series resonated at f_T with lumped elements. This would require a series negative capacitor in the case of the *K*- and *Ka*-band diodes. The negative Q values are computed using the formula:

$$Q = (f_T/2R_d) \cdot (dX/df) \tag{4}$$

where R_d is the value of negative resistance and dX/df is the reactance slope at f_T. These low values of negative Q affirm that Gunn diodes are capable of high gain per stage (8 to 10 dB) over wide (octave) bandwidths.

The diode impedances discussed above are obtained at small-signal levels and are used to predict the linear gain response. In order for a Gunn reflection amplifier to deliver significant power, the device must be driven into its nonlinear region. An analysis of such nonlinear behavior of power amplifiers has been presented in the literature [13].

III. MATCHING NETWORKS FOR STABLE GUNN-EFFECT AMPLIFIERS

Negative resistance diodes such as the Gunn-effect diode can be utilized for stable negative resistance amplifiers if the real part of the circuit impedance is greater than the negative resistance of the device at all frequencies where the sum of the reactances becomes zero. A nonreciprocal device, such as a ferrite circulator, is utilized to separate the incident and reflected (amplified) waves. The matching networks which are included between the active device and the circulator must be designed to stabilize the diode and to present a reflection coefficient with constant amplitude to the circulator over the desired frequency range.

Transducer power gain for a reflection amplifier is given by:

$$G_t(\omega^2) = |\Gamma(j\omega)|^2 \tag{5}$$

where $\Gamma(j\omega)$ is the reflection coefficient at the diode defined by:

$$\Gamma(j\omega) = \frac{Z_c(j\omega) - Z_d^*(j\omega)}{Z_c(j\omega) + Z_d(j\omega)} \tag{6}$$

where $Z_d(j\omega)$ is the diode impedance, $Z_c(j\omega)$ is the circuit impedance as "seen" by the diode, and $Z_d^*(j\omega)$ is the complex conjugate of the diode impedance.

Stability requires that the denominator in (6) never vanish, and absolute stability is insured if the loci of Z_c and $-Z_d$ as plotted on a Smith chart do not intersect. Referring to Fig. 1, it follows that there is an area on the Smith chart, right or left of the $-Z_d$ locus, in which Z_c is permitted to fall. With increasing RF power, the Gunn-diode device line $-Z_d$ moves toward the left. Thus if the input impedance of the matching circuit is on the right side, absolute stability is insured at all drive levels.

Classical broad-banding techniques referenced above require the use of alternate series and shunt resonators as shown in lumped form in Fig. 2(a) for the case of two resonators. The first (series) resonator represents the resonated packaged diode. The transformer is generally necessary to set the desired midband gain, and the shunt resonator has the function of broad-banding the response. If the broad-banding resonator is realized as a shorted quarter wavelength stub at band center, the locus of Z_c will intersect $-Z_d$ at two frequencies, which in all likelihood, would lead to instabilities.

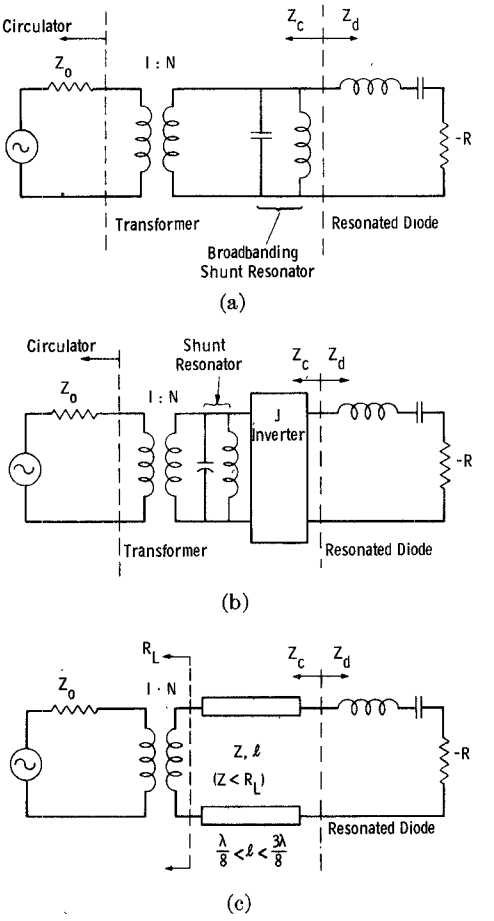

Fig. 2. Matching network equivalent circuits. (a) Classical broadband matching circuit with shunt resonator adjacent to the resonated device. (b) Inverted shunt resonator adjacent to the resonated device. (c) Short length of transmission line adjacent to resonated device. The circuits in (b) and (c) are examples of series resonant matching networks desirable for stability.

The objective of this work is to design relatively narrow-band (5–10 percent) amplifiers for communication applications. Either a portion of the bandwidth of a broad-band amplifier [13], [14], or a narrow-band circuit design can be used. In many cases, the second approach is dictated because of the out-of-band characteristics of other components in the amplifier. A narrow-band amplifier design is achieved with the use of a series resonator adjacent to the diode.

If it becomes impractical to fabricate a series resonator directly, such as in the microstrip medium, it is possible to achieve its equivalent by inverting a shunt resonator, which is easier to realize [see Fig. 2(b)]. This circuit forms the basis for the designs used in the X- and Ku-band Gunn amplifiers, which will be explained in the next section.

Another interesting way of creating circuits which exhibit series resonance behavior has been treated by Upadhyayula and Perlman [6], who introduced matching networks utilizing transmission lines. The basic building block is a section of resistively terminated transmission

line. If the characteristic impedance Z of the line is smaller than the load resistance R_L, the resistive part of the input impedance is always greater than Z^2/R_L. In this case, the reactive part exhibits a positive reactance slope over the frequency range for which $\lambda/8 < l < 3\lambda/8$, where l is the length of the transmission line section, and λ is the free-space wavelength. In particular, in the frequency range $\lambda/8 < l < \lambda/4$ where the reactance is capacitive, such a curcuit is ideally suited to be used with *Ka*-band diodes which are inductive in their operating frequency range. The equivalent circuit of such a network is shown in Fig. 2(c). The details of how this circuit was used in the design of *Ka*-band Gunn amplifiers are given in the next section.

IV. DESIGN OF MULTISTAGE GUNN-EFFECT AMPLIFIERS

Gunn amplifier stages can be cascaded to achieve high gains and, using isolators, stability can be maintained and stage interaction minimized. The organization of a typical two-stage Gunn-effect amplifier is shown in Fig. 3. The block diagram shows two circulator-coupled Gunn-effect amplifier stages, preceded by an isolator at the input, which reduces the input VSWR (operating) from greater than 2:1 to less than 1.3:1. An output isolator has a similar effect on the output VSWR and protects the output stage from becoming unstable due to large load mismatches.

A. Design of Single Stage for the X- /Ku-band Amplifiers

A small-signal single-stage gain of approximately 10 dB is required over the frequency ranges of 11.7 to 12.2 GHz and 14.0 to 14.5 GHz. A number of factors are considered important in the overall amplifier design. Small active circuit size is deemed very important for two reasons, the physical size of the total amplifier should be kept small and the electrical length should be minimized for better group delay performance. Reproducibility and ease of tuning are also important factors in the design of the circuits. For these reasons, a microstrip circuit configuration is decided upon.

It is desirable to have a direct circuit interface with the circulator to eliminate transitions and a separate launcher. A microstrip circuit also simplifies the bias circuit design problems.

The amplifier design was initiated with two circuits, a straight 50-Ω line and a three-step 50–75-Ω wide-band transformer with a bandwidth of 3:1 centered at 12 GHz. The Gunn diodes had 30 Ω maximum negative resistance and were capacitive over most of the frequency range as shown in Fig. 1 for the *X*-band diode. These circuits were evaluated in conjunction with the above-mentioned diodes, and it was found that they could not be stabilized at any bias voltage up to and including 14 V. Oscillations occurred at frequencies outside the band of interest. Upon closer examination of the circuit, it was recognized that parasitic end effects caused the circuit and device lines to cross and cause instability. Such instabilities have been described [16].

It was realized that a series resonant circuit of the type

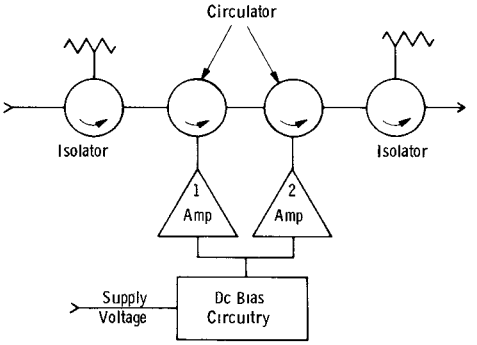

Fig. 3. Organization of a two-stage Gunn-effect amplifier.

described in Section III was needed. Since it is impractical to realize a series resonator in microstrip, it was decided to resort to inverting a shunt resonator in the form of a $\lambda/4$ shorted stub. This inverting process has been described by McDermott and Levy [17], who reported a variation of the Kuroda technique. If an impedance inverter is used preceding a $\lambda/4$ shunt short-circuited stub followed by a resistive load, then the input impedance of this cascade is electrically equivalent to a series resonant circuit.

The $ABCD$ matrix $[A_1]$ of an impedance inverter with $+90°$ image phase shift and inverter impedance Z_i is

$$[A_1] = \begin{bmatrix} 0 & jZ_i \\ j/Z_i & 0 \end{bmatrix}. \tag{7}$$

The $ABCD$ matrix $[A_2]$ for a shunt short-circuited stub of admittance Y_s and electrical length θ is

$$[A_2] = \begin{bmatrix} 1 & 0 \\ -jY_s \cot\theta & 1 \end{bmatrix} \tag{8}$$

If the circuits are cascaded and terminated with a load resistance R, then the input impedance of the inverter-shunt stub-load resistor combination is

$$Z_{IN} = \frac{Z_i^2}{R} - \frac{jZ_i^2 \cdot \cot\theta}{Z_s} \tag{9}$$

where $Z_s = 1/Y_s$.

Thus Z_{IN} looks like a series circuit since the real part is constant as a function of frequency, and the imaginary part tends to 0 for $\theta = \pi/2$. The inverter was designed using distributed circuits by the procedures reported by Davis and Khan [18]. The image phase shift was chosen to be $+90°$ since negative lengths of line could not be accommodated in the design.

The inverted shunt circuit is shown in Fig. 4(a). The parasitic elements represent the inductance of the bonding wire connecting the diode and substrate and the capacity of the microstrip fringing capacitance. The basic physical layout of the circuit, including bias lines and impedance transformers, is shown in Fig. 4(b). Circuits were constructed on 0.025-in alumina substrates 0.5×0.5 inches in size. The finished circuit was 0.5×0.75 in, including the heat sink.

The predicted gain response and the real parts of both

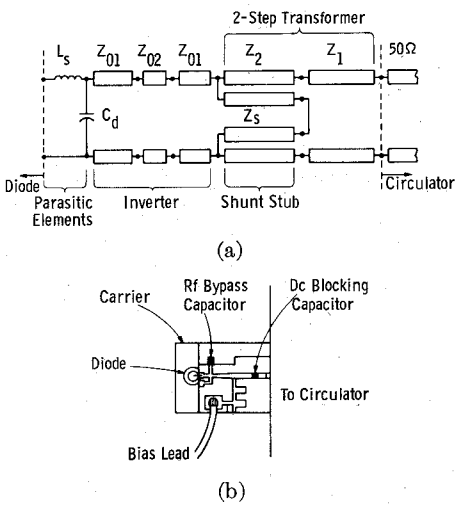

Fig. 4. Inverted shunt circuit. (a) Circuit design. (b) Physical layout including bias lines and blocking capacitors.

diode and circuit impedance are shown in Fig. 5. It can be seen that indeed the real part of the circuit impedance exceeds the value of the negative resistance of the diode over the entire frequency range of 6 to 15 GHz. Initial test results on the amplifier circuits were very encouraging. Utilizing diodes which previously could not be stabilized, stable gain was achieved with a bias voltage of only 6.1 V. The actual gain response peaked slightly high in frequency (Fig. 5), due to overestimating the inductance of the bonding wire. Upon increasing the length of the bonding wire, the gain response was precisely centered. Very little interaction was noticed between stages when two pretuned stages were operated in cascade on a 4-port circulator.

B. X/Ku Amplifier Performance

Small-signal gain, phase deviation, and group delay data of the finished two-stage *X*-band amplifier are presented in Fig. 6. The average small-signal gain is 18.4 dB. A ±0.4-dB gain variation is observed. The time delay is 2.2 ns and the maximum deviation from linear phase slope is +4.1° at the lower bandedge. The center band deviation is ±2.3°. The maximum delay distortion is of 0.02 ns/10 MHz.

The large-signal characteristics are summarized by a saturated power output of +23 dBm and third-order intermodulation (3-IM) intercept of +26 dBm. The 1-dB compression point is at −5-dBm power. No distortion of the amplifier passband is observed up to input levels of +15 dBm and no gain expansion is observed. The noise figure is found to be 23.2 dB. Small-signal gain variation with temperature is ±0.75 dB maximum from 0°C to 50°C with no temperature compensating networks in the dc bias circuit.

The performance of the two-stage *Ku*-band 14.0 to 14.5 GHz amplifier is quite similar to the *X*-band unit. The *Ku*-band unit has less phase deviation from linear (3.2° max), but slightly larger delay distortion (0.03 ns/10 MHz) and gain variation (±0.49 dB).

Both amplifiers require 1.5 A at 14 V, including the regulator. Dimensions are 2 × 3 × 4.5 in and input/output

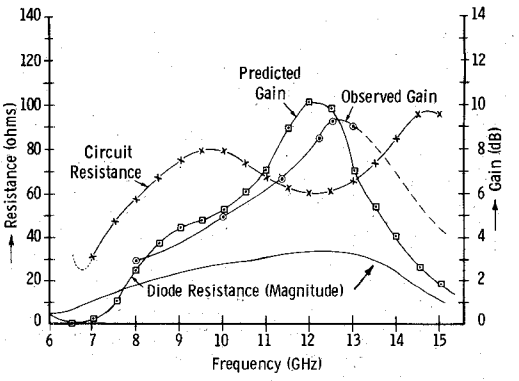

Fig. 5. Predicted and measured gain for the circuit shown in Fig. 4 Also shown are the magnitudes of the real parts of the diode and circuit impedances.

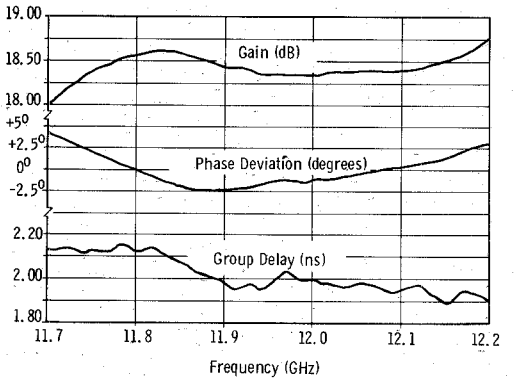

Fig. 6. Small-signal gain, deviation from linear phase, and group delay for the two-stage *X*-band amplifier.

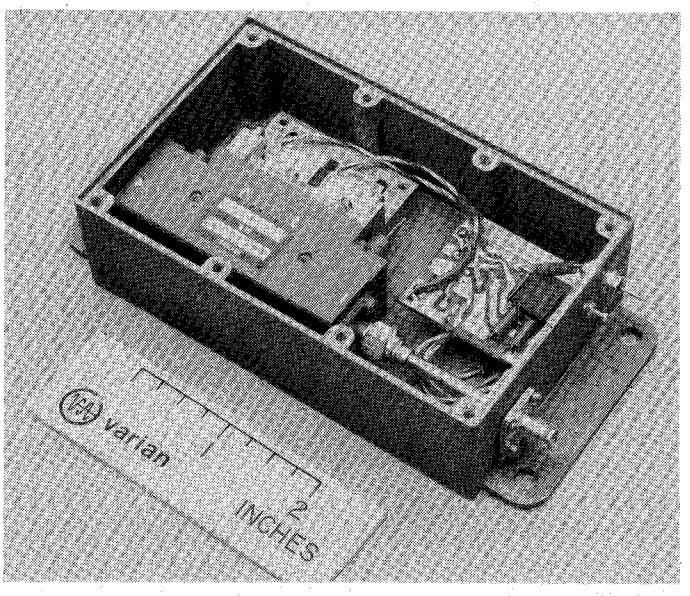

Fig. 7. Two-stage *X*-band amplifier in final package.

connectors are SMA type. Weight is about 1.5 lb. The finished *X*-band amplifier is shown in Fig. 7.

C. Single-Stage Amplifier Design for Ka-band

1) Basic Circuit Design: The design of the single-stage amplifier in high *Ka*-band is based on the *Ka*-band Gunn diode impedance characteristics in Section II and the general circuit approach outlined in Section III. The

objective of the design of the matching network is to provide the desired stable gain over the required frequency range. The matching circuits are coaxial/waveguide hybrid structures [11]. The packaged diode is imbedded at the end of a coaxial line section, approximately 60°. A large semisection of the outer conductor is removed, with the removed section facing the waveguide opening to form a broad-band coaxial-to-waveguide transformer. A wide-band choke is used to terminate the opposite end of the line and to provide dc bias to the Gunn diode.

A simplified equivalent circuit for the frequency range of interest is shown in Fig. 8. The coaxial-to-waveguide transformer is represented by the ideal transformer. The circuit input impedance Z_c is shown on the Smith chart in Fig. 8; the solid dots are measured data, and the crosses indicate the input impedance data derived from the equivalent circuit. Also shown is the negative of the impedance of the packaged diode, mounted at the end of the coaxial line ($-Z_d$). The circles indicate observed and the squares indicate calculated impedance data.

In Fig. 9 the predicted and observed gain is shown for the diode circuit combination discussed above. A small-signal gain of 11 dB ± 0.5 dB is achieved over 36–40 GHz at 5 V and 0.7-A bias, and the observed gain curve follows the predicted gain response with good agreement.

The Gunn diodes used in this work were pretested in an oscillator test circuit at 35 GHz and found to exhibit the characteristics summarized in Table II.

2) Limitations Due to Ferrite Circulator: Measuring the gain on a waveguide reflectometer setup, a smooth response without ripples is observed. When operated with a ferrite circulator, several ripples appear across the passband due to mismatches from the circulator. By carefully matching the circulator, 26-dB return loss could be obtained over the band, and therefore the peak-to-peak small-signal gain variation can be kept as low as ±1.5 dB at the 10-dB nominal gain level.

Operating two nearly identical stages simultaneously on a multiport ferrite circulator, it is observed that the overall amplifier gain variation increases due to the fact that the gain peaks and valleys appear at the same frequency for both stages. Therefore, the electrical length between amplifier stage and circulator junction may be chosen differently for each stage in order to keep the overall gain variation low.

The out-of-band behavior of the circulator is also of importance. Due to the circulator, sharp resonances can occur outside the passband, and instabilities can arise. It is therefore necessary to specify the VSWR of the circulator to a frequency substantially higher than the upper frequency of the band, since it is generally not practical (particularly in *Ka* band) to design the matching networks with a sharp enough rolloff. Isolation must be specified outside the band of interest to avoid oscillations which may occur due to interaction between successive gain stages at out-of-band frequencies.

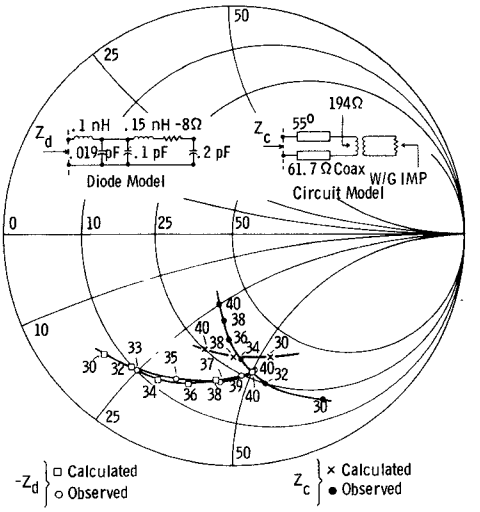

Fig. 8. Calculated and observed diode and circuit impedances and models used for diode and circuit impedance calculations in *Ka* band.

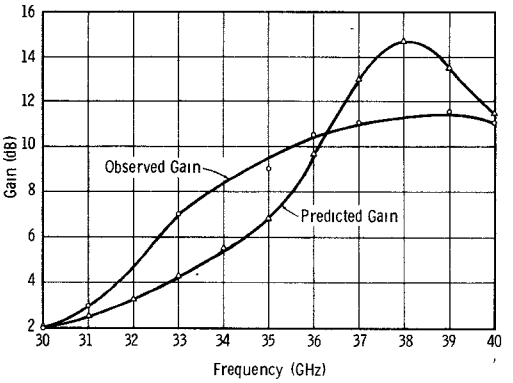

Fig. 9. Measured and computed gain for single-stage *Ka*-band reflection amplifier.

TABLE II
OSCILLATOR PERFORMANCE DATA OF *Ka*-BAND AMPLIFIER DIODES

Threshold voltage	15 – 16 V
Threshold current	1 A
Operating voltage	6.5 V
Operating current	0.85 A
Output power	125 mW
Efficiency	23 %

D. Multistage Ka-band Amplifier Performance

The latest advances with Gunn effect devices discussed here include the development of two dual-stage *Ka*-band amplifiers. The first provides 110-mW output power and 12 dB ± 0.25-dB gain over 36.2 to 38.6 GHz, and the second amplifier exhibits 13 dB ± 1 dB-gain at 100-mW minimum output power over the frequency range of 35.5 to 39.5 GHz. A four-stage amplifier exhibits 30-dB gain

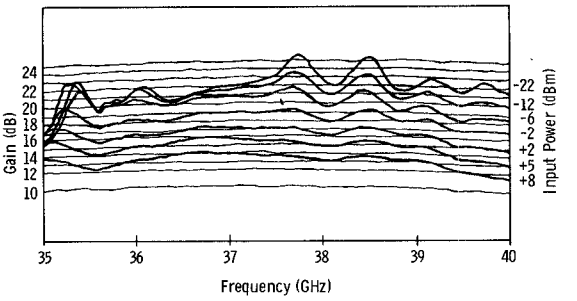

Fig. 10. Gain response as a function of input power for the wide-band two-stage amplifier in *Ka* band.

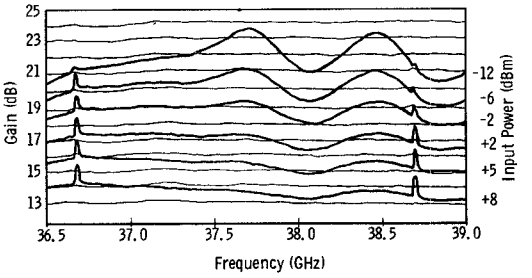

Fig. 11. Gain response as a function of input power of the amplifier of Fig. 10 over the narrower range of 36.7 to 38.7 GHz.

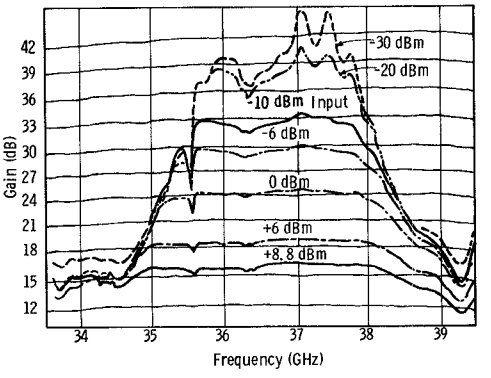

Fig. 12. Gain response as a function of input power for a four-stage *Ka*-band amplifier.

with 100-mW output over 35.7 to 37.2 GHz and has 250-mW saturated output power.

The block diagram and organization of these amplifiers are similar to the diagram given in Fig. 3. The frequency response of the two-stage 4-GHz bandwidth unit at input power levels ranging from −22 dBm (small signal) to +8 dBm (rated input) for constant bias voltage is shown in Fig. 10. The small-signal gain is 23 ± 3 dB over the entire frequency range of 35.5 to 39.5 GHz. Note that the compression characteristics are smooth with no observable gain expansion at low-drive levels. No detuning of the passband has been observed at drive levels from −22 dBm to +8 dBm.

Fig. 11 shows a family of gain response curves at input levels varying from −12 dBm to +8 dBm over the narrower frequency range of 36.75 to 38.75 GHz. Gain variation is less than ±1.25 dB for all drive levels. The amplifier noise figure, measured utilizing the standard *Y*-factor method, is 20.4 dB. The power consumption of the two-stage unit is 9 V and 1.9 A, including the voltage regulator. Excluding the regulator, the generation efficiency (P_{add}/P_{dc}) is 1.4 percent at 130-mW output. Size of the finished two-stage unit with integral power supply is 4.0 × 2.5 × 1.5 in excluding the mounting flanges, and the weight is 1 lb., 7 oz. Similar two-stage amplifiers have exhibited ±1° phase deviation from linear over 200 MHz and less than 5°/dB AM–PM conversion at rated output of 130 mW.

The frequency response of the four-stage amplifier at different input power levels is shown in Fig. 12. The

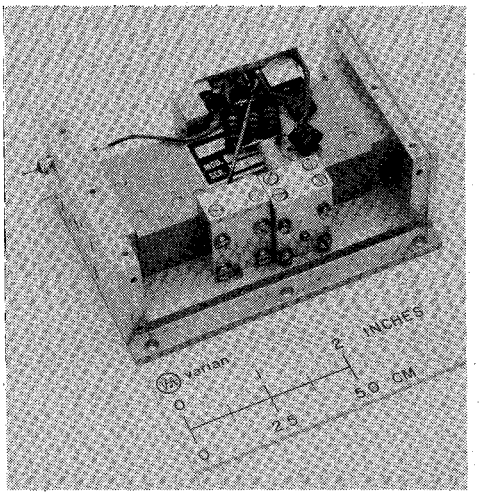

(a)

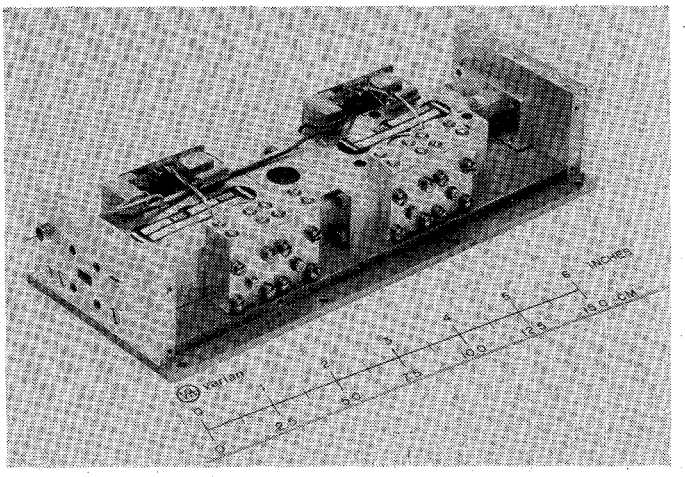

(b)

Fig. 13. *Ka*-band amplifiers. (a) Two stage. (b) Four stage.

figure indicates 33-dB gain at −10-dBm input power, with ±1 dB-large-signal variation and 6–10-dB compression. Again exceptionally smooth saturation behavior is indicated, with no detuning or gain expansion. Saturated output power is approximately 250 mW. The output power decreased by 1.0 dB at the high-frequency end of the band as the baseplate temperature was increased from 25°C to 60°C. Third-order intermodulation distortion has been measured at two frequencies in the band and the 3-IM intercept was calculated to be 2 dB above the saturated power output at both frequencies. At the 1-dB compression point, the 3-IM products were down 18 dB and at rated power, 15 dB. Power consumption, including regulators, was 10 V and 3 A. Fig. 13 shows both the wide-band two-stage and the four-stage *Ka*-band amplifiers.

V. CONCLUSIONS

In conclusion, when series resonant matching structures are used in conjunction with Gunn diodes, narrow-band stable amplification results. These amplifiers are appropriate for use in communication systems. It is also shown that this approach can be utilized with the microstrip medium at microwave frequencies and with coaxial/waveguide hybrid structures at millimeter wave frequencies.

Cascading a number of individually stable reflection stages, higher gain levels can be attained. *X*- and *Ku*-band microstrip amplifiers have demonstrated flat linear gain with flat phase and large third-order modulation intercept. *Ka*-band amplifiers have yielded high gain with low distortion at medium power levels with smooth saturation characteristics.

These Gunn amplifiers have been developed as drivers for high-power transmitters in microwave communications systems. Gunn amplifiers with their inherent long lifetime and low-supply voltage offer attractive alternatives to tube amplifiers up to 1 W. Higher output powers and lower noise figures, as well as developments beyond 40 GHz, are anticipated.

REFERENCES

[1] H. W. Thim and M. R. Barber, "Microwave amplification in a GaAs bulk semiconductor," *IEEE Trans. Electron Devices*, vol. ED-13, pp. 110–114, Jan. 1966.
[2] H. W. Thim and H. H. Lehner, "Linear millimeter wave amplification with GaAs wafers," *Proc. IEEE* (Lett.), vol. 55, pp. 718–719, May 1967.
[3] S. Y. Narayan and F. Sterzer, "Stabilization of transferred electron amplifier with large N_0l products," *Electron. Lett.*, vol. 5, pp. 30–31, Jan. 1969.
[4] B. S. Perlman, C. L. Upadhyayula, and R. E. Marx, "Wide-band reflection-type transferred electron amplifiers," *IEEE Trans. Microwave Theory Tech.*, vol. MTT-18, pp. 911–921, Nov. 1970.
[5] B. S. Perlman, C. L. Upadhyayula, and W. W. Siekanowitz, "Microwave properties and application of negative conductance transferred electron devices," *Proc. IEEE*, vol. 59, pp. 1229–1237, Aug. 1971.
[6] C. L. Upadhyayula and B. S. Perlman, "Design and performance of transferred electron amplifiers using distributed equalizer networks," *IEEE J. Solid-State Circuits*, vol. SC-8, pp. 29–36, Feb. 1973.
[7] A. Séne and F. J. Rosenbaum, "A wide-band Gunn-effect CW waveguide amplifier," *IEEE Trans. Microwave Theory Tech.*, vol. MTT-20, pp. 645–650, Oct. 1972.
[8] M. Omori, "Injection controlled negative resistance amplifier in GaAs," presented at the IEEE Device Research Conf., Ann Arbor, Mich., June 1971.
[9] A. A. Sweet, J.-C. R. Collinet, and R. N. Wallace, "Multistage Gunn amplifiers for FM–CW systems," *IEEE J. Solid-State Circuits*, vol. SC-8, pp. 20–28, Feb. 1973.
[10] S. Baskaran and P. N. Robson, "Gain and noise figure of GaAs transferred electron amplifiers at 34 GHz," *Electron. Lett.*, vol. 8, pp. 109–110, Mar. 1972.
[11] S. Baskaran and P. N. Robson, "Noise performance of InP reflection amplifiers in *Q*-band," *Electron. Lett.*, vol. 8, pp. 137–138, Mar. 1972.
[12] R. E. Goldwasser and F. E. Rosztoczy, "35 GHz transferred electron amplifiers," *Proc. IEEE* (Lett.), vol. 61, pp. 1502–1504, Oct. 1973.
[13] M. E. Hines, "Negative-resistance diode power amplification," *IEEE Trans. Electron Devices*, vol. ED-17, pp. 1–8, Jan. 1970.
[14] W. J. Getsinger, "Prototypes for use in broadbanding reflection amplifiers," *IEEE Trans. Microwave Theory Tech.*, vol. MTT-11, pp. 486–497, Nov. 1963.
[15] G. L. Mattheai, L. Young, and E. M. T. Jones, *Design of Microwave Filters, Impedances, Marching Networks and Coupling Structures*. New York: McGraw-Hill, 1964, pp. 135–144 and 714–719.
[16] J. W. Monroe, "The effects of package parasitics on the stability of microwave negative resistance devices," *IEEE Trans. Microwave Theory Tech.*, vol. MTT-21, pp. 731–735, Nov. 1973.
[17] M. M. McDermott and R. Levy, "Very broadband coaxial DC returns derived by microwave filter synthesis," *Microwave J.*, vol. 8, pp. 33–36, Feb. 1965.
[18] W. A. Davis and P. J. Khan, "Coaxial bandpass filter design," *IEEE Trans. Microwave Theory Tech.*, vol. MTT-19, pp. 373–380, Apr. 1971.